Gravity-Driven Remediation of DNAPL Polluted Aquifers using Densified Biopolymer Brine Solution

Amir Alamooti, Stéfan Colombano, Dorian Davarzani, Fabien Lion, Azita Ahmadi-Sénichault

HAL Id: hal-04449753
https://brgm.hal.science/hal-04449753

Submitted on 9 Feb 2024

Gravity-driven remediation of DNAPL polluted aquifers using densified biopolymer brine solution

Amir Alamooti [a,b,c,d,*], Stéfan Colombano [a], Dorian Davarzani [a], Fabien Lion [a], Azita Ahmadi-Sénichault [b,c]

[a] *BRGM (French Geological Survey), Orléans 45060, France*
[b] *CNRS, Bordeaux INP, I2M, UMR 5295, University of Bordeaux, Talence F-33400, France*
[c] *Arts et Metiers Institute of Technology, I2M, UMR 5295, CNRS, Bordeaux INP, Hesam Universite, Talence F-33400, France*
[d] *ADEME (French Environment and Energy Management Agency), Angers 49004, France*

ARTICLE INFO

ABSTRACT

Polymer solutions aid DNAPL (Dense Non Aqueous Phase Liquid)-contaminated soil remediation but are impacted by gravity and viscous forces. This study assesses the interplay between buoyancy and viscous forces in influencing the distribution of DNAPL and the invading phase, by introducing a densified brine (NaI) biopolymer (xanthan) solution as remediation fluid. A matrix of experiments was conducted, encompassing rheological measurements, multiphase flow tests in 1D-columns and 2D-tanks. Numerical modeling was used to assess polymer and DNAPL propagation under different conditions. NaI addition maintains xanthan's shear-thinning yet lowers mid-range shear viscosity 2.6 times. Confined column tests show similar 89 % performance for viscous polymer solutions regardless of density. Unconfined tests mimicking real sites reveal non-densified viscous polymer solution yield mere 0.09 recovery due to density-driven flow. Densified polymer attains radial invasion, boosting recovery to 0.46 with 1.21 aspect ratio. Numerical simulations aligned with experiments, suggesting a near-zero gravity number is necessary to prevent density-driven flow problems. The multiphase flow experiments in confined multilayer system are performed and using the numerical modeling the effects of the permeability contrast and dimensions of the layers on the shape of front are analyzed.

1. Introduction

Spills of heavy chlorinated solvents (DNAPL) through the soils is one of the main environmental issues in many industrial sites (Alamooti et al., 2022; Colombano et al., 2020; Maire et al., 2019; Santos et al., 2018). DNAPLs can penetrate through the soil and form polluted pools under the groundwater level due to gravity forces (Taghavy et al., 2010; Yang et al., 2020). Several advanced technologies including surfactant injection (Lee et al., 2005; Pennell and Abriola, 2017; Walker et al., 2022), foam injection (Fitzhenry et al., 2022; Longpré-Girard et al., 2020; Maire et al., 2019) and polymer injection have been developed for the remediation of DNAPL polluted soils (Alamooti et al., 2022, 2023, 2024, ; Martel et al., 1998; Omirbekov et al., 2023). However, the efficiency of these methods for DNAPL remediation can be limited as the density-driven flow affects the recovery of DNAPL. During the remediation of soils contaminated with DNAPL, density-driven flow has been observed. This occurs when a less dense fluid displaces a denser fluid,

known as overridden flow, or when a denser fluid displaces a less dense fluid, known as underridden flow. Several studies have investigated density underridden flow in 2D systems for DNAPL remediation purposes, including miscible cosolvent displacement by water injection (Jawitz et al., 1998; Taylor et al., 2001), and water displacement during brine surfactant injection (Zhong et al., 2008). Zhong et al. (2008) proposed that the addition of the polymer to the densified brine surfactant can control the underriden flow by providing enough viscous forces to overcome gravity; however, the relative density difference has been limited to 1.008. Taylor et al. (2004) in a set of two dimensional experiments observed that a minor density difference (0.008 g/mL) between the injecting ethanol-surfactant mixture and water present near the perchloroethylene (PCE)-contaminated zone can result in density overridden flow. Grubb and Sitar (1999) reported the downward migration of trichloroethylene (TCE) along the water-ethanol interface during ethanol injection in two-dimensional uniform and layered sand packs. They also observed the ethanol gravity override with an

---

increasing inclination angle of the ethanol front along with invasion progress. The density difference between ethanol and water is 0.211 g/mL, and the density difference between TCE and water is 0.46 g/mL.

Density modification displacement is an approach to control the downward migration of DNAPL by reducing its density through sufficient partitioning of alcohol within DNAPL and turning it to LNAPL (Damrongsiri et al., 2013; Kibbey et al., 2002; Lunn and Kueper, 1999; Ramsburg and Pennell, 2002). The density modification by alcohol partitioning can be reversible depending on the equilibrium of alcohol, water and DNAPL (or newly formed LNAPL). Besides, colloidal biliquid aphron (CBLA), consisting of two surfactants, water, and an oil phase, has been employed to control the downward migration of DNAPL to non-polluted zones by lowering its density (Yang et al., 2020; Yan et al., 2011). CBLA has a foam structure with micron-sized (5–20 μm) droplets consisting of an outer thin aqueous phase and an internal light organic phase. In this approach, the internal light non-aqueous phase is mixed with DNAPL using a demulsifying agent, which transforms it into Light Non-Aqueous Phase Liquids LNAPL. Although it can influence the downward migration of DNAPL, its efficiency relies on the performance of the demulsifier. Also, propagation of the light colloidal biliquid aphron that can flow over the DNAPL is challenging due to the influence of buoyancy forces.

To mobilize a DNAPL droplet trapped in pore spaces, the summation of the buoyancy and viscous forces should be more than capillary force (Alamooti et al., 2020; Mansouri-Boroujeni et al., 2023; Pennell et al., 1996). The gravity number is defined as the ratio of the buoyancy and viscous forces showing the balance between them and consequently the direction of flow. It can be considered as (Shook et al., 1998):

$$N_G = \frac{\Delta \rho g k}{v \mu} \tag{1}$$

where $\Delta \rho$ is the density difference (kg/m^3), g is the gravitational acceleration (m/s^2), k is the intrinsic permeability (m^2), v is the velocity magnitude of the invading phase (m/s), μ is the viscosity of the invading phase (Pa s). Large negative N_G values correspond to dominant buoyancy forces leading to a vertical migration of the DNAPL if the residence time of the injected phase is large as well (Jin et al., 2007).

Miller et al. (2000) in an experimental study used a brine (sodium iodide dissolved in water) solution with a density of 1.79 g/mL to displace the DNAPL (TCE with a density of 1.464 g/mL) pools in a two-dimensional heterogeneous system. They showed that using the densified brine solution around 55 % of initial DNAPL was recovered as a direct result of buoyancy forces, however the residual DNAPL was distributed in the entire medium. Jin et al. (2007) in a numerical study examined the downward migration of DNAPL during surfactant flooding. In their numerical approach they considered negligible adsorption of chemical species and dispersion in the transport; focusing mainly on `body forces' i.e. viscous, buoyancy, and capillary forces. The simulation outcomes indicated that there is a high risk of DNAPL's downward migration during surfactant flooding if the viscous forces are not dominant. This highlights the crucial role played by viscous forces, which can be supplied by the polymer solution.

The performance of the injection of the polymer solutions for recovery of pollutants in contaminated soils have been widely investigated (Alamooti et al., 2022; Bouzid and Fatin-Rouge, 2022; Giese and Powers, 2002; Martel et al., 1998, 2004; Omirbekov et al., 2023; Robert et al., 2006; Wu et al., 2000).

Robert et al. (2006) evaluated density-driven plume sinking during the injection of a xanthan-surfactant mixture for displacement of TCE in a heterogeneous 2D sandbox. Their results indicated that to prevent downward migration of surfactant polymer mixture containing the dissolved DNAPL, it is important to avoid excessive increase in the density of the mixture during DNAPL dissolution. They stated that the density plume sinking can be prevented by a strong hydraulic gradient that can be provided by a polymer.

Recent studies have shown that the injection of a densified polymer suspension can improve up to four times the recovery of a multicomponent DNAPL compared to a non-densified polymer solution (Alamooti et al., 2022; Omirbekov et al., 2023). Alamooti et al. (2022) conducted numerical and experimental investigations, revealing that densifying the polymer (carboxymethyl cellulose) with barite particles to match the DNAPL density (same DNAPL as in this study) can counteract buoyancy forces and improve DNAPL recovery. The lateral displacement of DNAPL decreased as the density of the barite-polymer suspension decreased. The study showed that the presence of barite particles in the polymer suspension can reduce soil permeability by up to 70 % due to barite particle deposition. While the presence of barite particles in the polymer suspension can reduce the back-diffusion of residual DNAPL to the groundwater zone, it can result in higher injection pressures and hinder the ability of subsequent remediation reagents to fully react with DNAPL.

In addition to studies about density-driven flow in the context of soil remediation, substantial research has investigated this phenomenon within porous media, commonly known as gravity currents (Anderson et al., 2003; Di Federico et al., 2014; Huppert et al., 2013; Longo et al., 2015). These currents play a crucial role in various environmental scenarios, such as seawater intrusion in coastal aquifers, where they manifest at the interface of fresh water and brine (Koohbor et al., 2019). This process is also observed in applications like CO_2 sequestration, where the interaction between CO_2-rich brine and CO_2-free brine induces natural convection. This, in turn, leads to the descent of dense CO_2-rich brine fingers under gravity, facilitating the transport of aqueous CO_2 into deep saline aquifers (Du et al., 2023). The propagation of density driven flow in natural porous formations is strongly affected by heterogeneity. In a theoretical study, density-driven fluid drainage from an edge of a heterogeneous system, exemplified by a V-shaped Hele-Shaw cell where permeability varies transverse to the flow direction, reveals that profile shapes and the remaining mass in the medium are influenced by variations in both vertical porosity and permeability (Zheng et al., 2013). Ciriello et al. (2013) developed an analytical formulation to describe the propagation of plane viscous gravity currents in porous media, considering varying permeability conditions transverse or parallel to the propagation direction. Their study reveals that spatial variations in permeability not only influence the rate of spreading but also affect the current profile, steepness, and average height.

Huppert et al. (2013) investigated the gravitational flow of a dense fluid in a two-layered porous medium, considering experimental and theoretical analyses. When the upper layer is more permeable than the lower one, gravity and flow focusing initially counteract. At low input flux, flow confines to the lower layer; however, beyond a critical flux, the fluid preferentially spreads horizontally in the upper layer before draining back down. Above this critical flux, increased resistance in the higher permeability upper layer dominates, causing the denser current to override the less dense fluid in the lower layer, leading to a gravitationally unstable state susceptible to Rayleigh–Taylor instability.

Di Federico et al. (2014) formulated a closed-form solution for radial gravity currents involving power-law fluids in porous media with deterministic vertical permeability variation. Their results highlight the substantial impact of the rheological properties of the intruding fluid and permeability variations on the radius and profile of gravity-driven currents within porous media.

In this work, we analyze the efficiency of the injection of a densified polymer brine solution to remediate the DNAPL-contaminated soil. This solution contains xanthan gum as the polymer and sodium iodide salt as a soluble densifier. We conducted several experiments, including rheological measurements, 1D column tests, unconfined single layer and confined two-layer 2D sandbox experiments aimed at investigating the impact of saline densification on DNAPL recovery efficiency. Additionally, we employed numerical simulations to assess the propagation of the polymer solution and DNAPL under various gravity numbers.

The main objectives of this study are (i) to assess the individual and

combined effects of increasing viscosity and densification of remediation fluid on the displacement of DNAPL, (ii) to compare the efficiency of these technologies in both confined 1D and unconfined 2D media, (iii) to analyze the competition between buoyancy and viscous forces on the distribution of DNAPL and the invading phase and (IV) to evaluate the efficiency of densified polymer solution on displacement of DNAPL from

two-layer system. This study aims to make a valuable contribution to the remediation of DNAPL contamination in groundwater environments.

Sand saturated with water, grain size: 0.6-0.8 mm
Sand saturated with DNAPL at residual water saturation; grain size: 0.6-0.8 mm

(a)

(b)

Sand saturated with DNAPL at residual water saturation, grain size: 0.4-0.6 mm
Sand saturated with DNAPL at residual water saturation; grain size: 0.2-0.3 mm
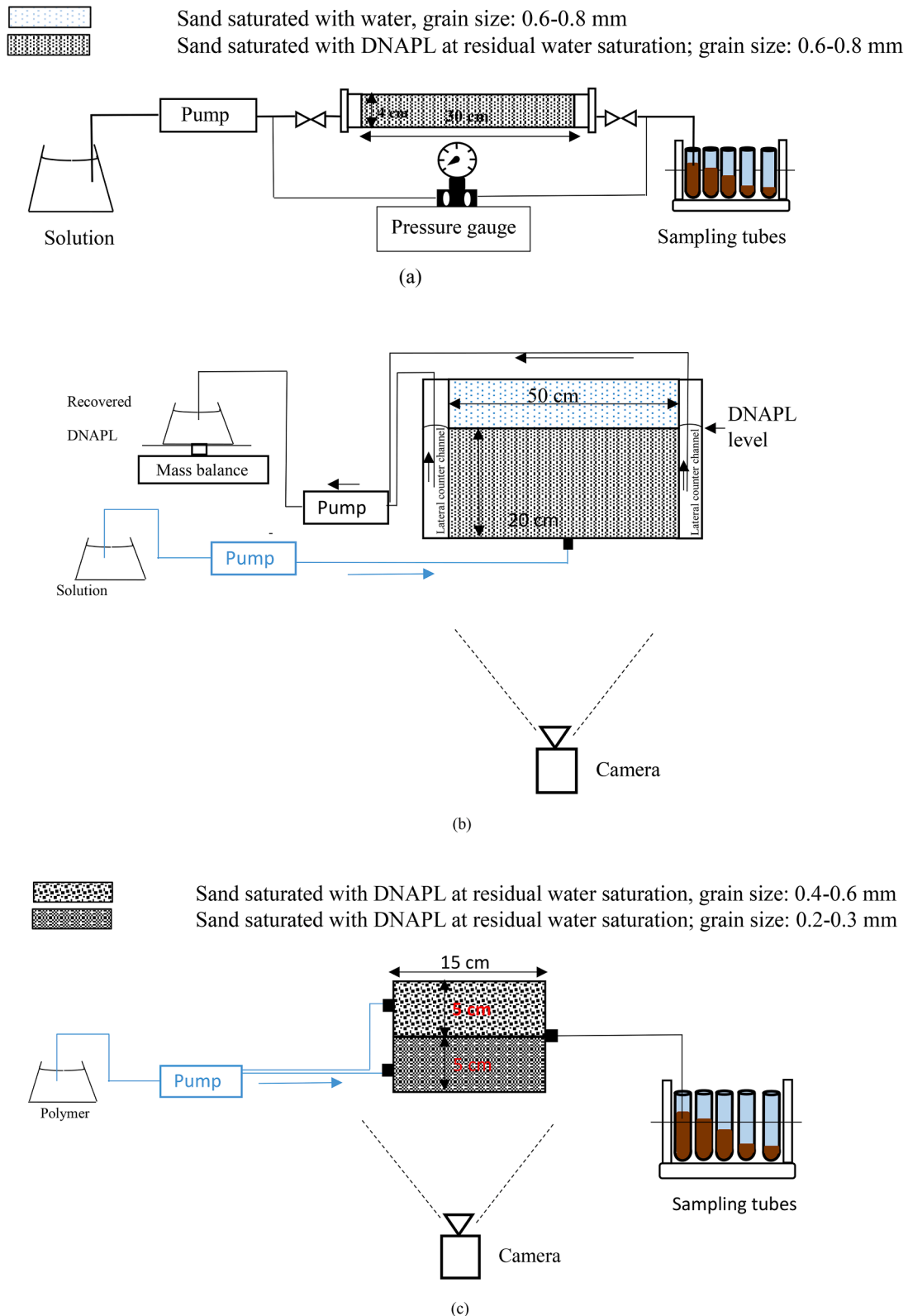
(c)

Fig. 1. Schematic of polymer-DNAPL displacement experimental setup. (a) 1D column setup, (b) unconfined 2D tank, and (c) confined multilayer 2D tank.

2. Materials and methods (experimental and numerical)

2.1. Experimental materials

The soil used in this study was made up of marble sand packs that were sieved and washed with deionized water, and then dried at a temperature of 105 °C. Three particle-size fractions of marble sand (0.2 to 0.3 mm, 0.4 to 0.6 mm, and 0.6–0.8 mm equivalent to absolute permeabilities of 0.34 ± 0.05, 1.05 ± 0.1, and 1.8 ± 0.1 0.10^{-10} m^2 respectively) have been used as the solid phase in 1D column and 2D tank studies.

Xanthan gum, a biopolymer with the chemical formula $C_{35}H_{49}O_{29}$ (purity >99 %), and sodium iodide salt (NaI) (purity >99 %) were provided in powder by Sigma-Aldrich, and solutions were prepared using deionized water. The DNAPL used in the study consisted primarily of hexachlorobutadiene-HCBD (58 %), hexachloroethane-HCA (14 %), and penta-chlorobenzene (3.5 %), as well as carbon tetrachloride (4 %). There are some other components in DNAPL mixture that are not quantifiable. The density and viscosity of the multicomponent DNAPL have been 1.66 g/mL and 4.47 mPa s, respectively (Alamooti et al., 2022; Colombano et al., 2020; Rodrigues et al., 2017). A rotational rheometer Haake Mars 60 equipped with the cone-plate geometry was used to assess the rheological behavior of the polymer solutions. Acknowledging the potential impact of wall slip on polymer rheology (Di Federico et al., 2017), we varied the gap between rotating and fixed plates, yet observed no significant changes in rheological behavior at different gap distances. The drop shape analyzer apparatus (DSA-100, KRUSS) was employed to measure the interfacial tension (IFT) between the polymer solutions and DNAPL. The IFT was determined using the pendant drop method at ambient temperature (22 ± 1 °C).

2.2. Column and 2D tank experiments

Column experiments were conducted to investigate the displacement of DNAPL by various solutions in a one-dimensional (1D) system. The experimental procedure, as described previously by Alamooti et al. (2022), involved using glass columns that were 4 cm in diameter and 30 cm in length. The columns were flushed with CO_2 gas, and then vertically saturated with deionized water at a flow rate of 0.1 mL/min for 2 PV. Next, DNAPL was injected vertically upward into the column at a flow rate of 1 mL/min until no water production was observed. Finally, the solutions were individually horizontally injected into the columns at a flow rate of 1 mL/min using a Reglo ICC digital peristaltic pumps (Ismatec®). The pressure at the inlet and outlet were monitored. A schematic of the multiphase flow in the 1D column experiments can be seen in Fig. 1a.

The unconfined 2D experiments were conducted to assess the efficiency of DNAPL displacement using different solutions in a system close to the real polluted site. The experiments were carried out in a 2D sandbox measuring 50 cm in length, 30 cm in height, and 2 cm in thickness. Initially, sand packs were compacted under water, and then DNAPL was injected into the water-saturated porous media until it reached a height of 20 cm. Next, different solutions were individually injected into the DNAPL-contaminated zone using a port located in the bottom central part of the sandbox at a flow rate of 2 mL/min. The level of DNAPL in the system was maintained constant during the injection of remediation fluids using peristaltic pumps connected to cavities on two sides of the sandbox. The injection of the solutions were continued until no more DNAPL was recovered or the solution fronts reached the lateral boundaries of the system. The mass of the recovered DNAPL was measured using a mass scale (Sartorius Cubis MSE8201S-000-D0), and real-time data (pressure and mass balance) acquisition was performed. To further analyze the propagation of the fluids, 2D images of the tank were regularly captured using a Nikon D810 camera equipped with a NIKKOR 105 lens. A schematic of the multiphase experiments in the unconfined 2D sandbox can be seen in Fig. 1b. This unconfined setup,

designed to mimic the fluid configuration of a real polluted site (featuring DNAPL-saturated soil at the bottom and water on top) and lacking confinement on the upper boundary, facilitates a clear visualization of how polymer solutions perform in displacing DNAPL within a polluted zone, notably without the presence of a blocking layer on top.

A confined 2D tank was used to evaluate the efficiency of injecting polymer solutions into a multilayer heterogeneous system. The tank's dimensions were 15 cm × 10 cm × 2 cm, with glass fronts for imaging. Two distinct layers, each 5 cm in height, were established within the tank, and sand was compacted inside, while water was continuously injected from the bottom. Upon complete saturation of the two layers with water, DNAPL was uniformly injected from three ports located at the bottom, through the layers, at a rate of 3 × 0.5 mL/min. Polymer solutions (un/densified) were injected from two ports on the left side of the tank at a rate of 2 × 0.5 mL/min. The injection of polymer led to the natural production of DNAPL in the effluent, similar to the column tests. The schematic of confined multilayer 2D tank is shown in Fig. 1c. This system facilitates monitoring the displacement of DNAPL, influenced by both permeability contrast and density differences, within a well-controlled multilayer porous media. It achieves this by preventing the vertical migration of the polymer solution (which is a scenario commonly observed in an unconfined 2D system).

2.3. Xanthan-NaI solutions

The concentration of xanthan in the polymer solution was chosen at 0.8 g/L to provide a stable front during displacement of DNAPL for the injection rate of 1 mL/min in the column (Lenormand et al., 1988). A dense brine solution was prepared by mixing sodium iodide with water to achieve a density close to that of DNAPL at 1.7 g/mL. The xanthan-NaI mixture was used to achieve the appropriate viscosity for a stable front, favorable mobility ratio, and to counteract buoyancy forces during DNAPL displacement. To prepare the mixture, the xanthan solution with a concentration of 0.8 g/L was initially prepared. Next, sodium iodide powder was added to the solution to reach a density of 1.7 g/mL, which is equivalent to a concentration of 960.11 g/L (considering the solubility of sodium iodide in water is around 1842 g/L at 25 °C). Consequently, the resulting mixture had a lower concentration of xanthan of 0.59 g/L. The descriptive parameters for each experiment is shown in Table 1.

2.4. Numerical modeling

2.4.1. Two-phase flow in porous media

The soil is considered as a uniform and isotropic porous medium containing water and DNAPL as incompressible and immiscible phases. The continuity equation for each phase can be considered as follows (Bear, 2013):

$$\frac{\partial}{\partial t}(\varnothing \rho_i S_i) + \nabla \cdot (\rho_i \boldsymbol{u_i}) = 0 \; with \; i = w, \; nw \tag{2}$$

where the subscripts "w" and "nw" refer to the wetting and non-wetting phases, respectively. The porosity is represented by the symbol $\varnothing$ (-), time by t (s), while the density, saturation, and the Darcy velocity of the i-phase are denoted by ρ_i(kg/m³), S_i (-) and $\boldsymbol{u_i}$ (m/s) respectively. The generalized Darcy's law for the flow of two phases in isotropic porous media is given by:

$$\boldsymbol{u_i} = -\frac{k \, k_{ri}}{\mu_i}(\nabla p_i - \rho_i \boldsymbol{g}) \tag{3}$$

where k (m²) represents the scalar absolute permeability of the isotropic porous medium, and k_{ri} (-) denotes the relative permeability for phase i. The viscosity and pressure of the phase i are represented by μ_i (Pa s), p_i (Pa) respectively, and the gravity vector is represented by $\boldsymbol{g}$ (m/s²). As the volume of the void space in a rigid porous medium is considered

Table 1
Parameters used in all experiments.

Dimensions D: diameter L: Length W: Width H: Height	Number of layers	Displacing phase	Displaced phase	$\Delta\rho \left(\frac{Kg}{L}\right)$ Displacing - Displaced	Injection rate (mL/min)	Grain size (mm)	Permeability (10^{-10} m^2)
1D column (D 4 cm × L 30 cm)	1	Xanthan	Water	0	1	0.6–0.8	1.8
1D column (D 4 cm × L 30 cm)	1	Xanthan-NaI	water	700	1	0.6–0.8	1.8
1D column (D 4 cm × L 30 cm)	1	Xanthan	DNAPL	−660	1	0.6–0.8	1.8
1D column (D 4 cm × L 30 cm)	1	Xanthan-NaI	DNAPL	34	1	0.6–0.8	1.8
1D column (D 4 cm × L 30 cm)	1	NaI	DNAPL	34	1	0.6–0.8	1.8
2D tank (L 50 cm × H 30 cm × 2 cm)	1	Xanthan	DNAPL	−660	2	0.6–0.8	1.8
2D tank (L 50 cm × H 30 cm × 2 cm)	1	Xanthan-NaI	DNAPL	34	2	0.6–0.8	1.8
2D tank (L 50 cm × H 30 cm × 2 cm)	1	NaI	DNAPL	34	2	0.6–0.8	1.8
2D tank (L 15 cm × H 10 cm × 2 cm)	2	Xanthan	DNAPL	−700	2 × 0.5	0.4–0.6	1.03
						0.2-0.3	0.34
2D tank (L 15 cm × H 10 cm × 2 cm)	2	Xanthan-NaI	DNAPL	34	2 × 0.5	0.4–0.6	1.03
						0.2-0.3	0.34

constant, it is exclusively occupied by aqueous and non-aqueous phases; therefore, the sum of the saturations of wetting and non-wetting phases always equals one. To present the capillary pressure, which reflects the difference in the pressure between the aqueous and non-aqueous phases, as well as the relative permeability curves in the model, Brooks and Corey functions are used (Brooks and Corey, 1964):

$$p_c = p_{th}S_{we}^{\frac{-1}{\lambda}} \tag{4}$$

$$k_{rw} = k_{rw}^{max}S_{we}^{\epsilon_w} \tag{5}$$

$$k_{rnw} = k_{rnw}^{max}S_{nwe}^{\epsilon_{nw}} \tag{6}$$

where the index of the pore size distribution is represented by λ (-) and p_{th} denotes the threshold pressure (Pa). The maximum relative permeability values, or end points, for the wetting and non-wetting phases are indicated by k_{rw}^{max} and k_{rnw}^{max}, respectively. ε_w and ε_{nw} indicate the saturation exponents for the wetting and non-wetting phases, respectively. The effective saturations of wetting and non-wetting phases are denoted by S_{we} (-) and S_{nwe} (-) and can be expressed as:

$$S_{we} = \frac{S_w - S_{wr}}{1 - S_{nwr} - S_{wr}} \tag{7}$$

$$S_{nwe} = \frac{S_{nw} - S_{nwr}}{1 - S_{nwr} - S_{wr}} \tag{8}$$

where the wetting irreducible and non-wetting residual saturations are represented by S_{wr} (-) and S_{nwr} (-), respectively.

2.4.2. Solute transport model

In porous media, the transport of solute is described by the classical differential advection-dispersion equation (O'Carroll et al., 2013; Tsakiroglou et al., 2018):

$$\underbrace{\frac{\partial(\varnothing S_w c_i)}{\partial t}}_{\text{Accumulation}} - \underbrace{\nabla\cdot(\varnothing S_w \boldsymbol{D}\cdot\nabla c_i)}_{\text{Dispersion}} + \underbrace{\boldsymbol{u_w}\cdot\nabla c_i}_{\text{Advection}} = R_i + \dot{m} \tag{9}$$

where the concentration of the i-component (kg/m^3) is represented by c_i, $\boldsymbol{D}$ denotes the dispersion tensor, the reaction term for the i-component is indicated by R_i and $\dot{m}$ signifies the source term. The adsorption of xanthan as an anionic polymer and NaI as an inherent tracer on the sand surface is neglected. The principal and cross terms of dispersion tensor for an isotropic porous medium can be represented as (Auset and Keller, 2004; Bear, 2013):

$$\boldsymbol{D} = \left(\propto_T |\boldsymbol{U_w}| + D_{eff}\right)\boldsymbol{I} + \left(\propto_L - \propto_T\right)\frac{U_{wx}U_{wy}}{|\boldsymbol{U}|} \tag{10}$$

$$D_{eff} = \frac{D_0}{\tau} \tag{11}$$

where the identity matrix is denoted as $\boldsymbol{I}$, the effective diffusion coefficient in porous media is represented as D_{eff} (m^2/s). The molecular diffusion coefficient is indicated as "D_0(m^2/s), and τ refers to the tortuosity. Furthermore, $\propto_L$ and $\propto_T$ are used to represent the longitudinal and transverse dispersivities, respectively.

Through the following formula, it is possible to derive the molecular diffusion coefficient of xanthan, a polysaccharide (Kono, 2014):

$$D_0 = 8.2 \times 10^{-9}Mw^{-0.49} \tag{12}$$

where the coefficient 8.2×10^{-9} is in (m^2 s^{-1} g$^{0.49}$ mol$^{-0.49}$) and Mw (g mol^{-1}) is the molecular weight of xanthan. Diffusion coefficients of sodium and iodide ions at 25 °C are 1.33×10^{-9} and 2×10^{-9} m^2/s, respectively (Yuan-Hui and Gregory, 1974).

By coupling the Eqs. (2), (3) and (9), the displacement of DNAPL and solute transport through two-dimensional domains was simulated. A total of 10,598 triangular meshes were used to discretize the simulation domain. The parameters used for simulating two-phase flow in 2D tank including the relative permeability, capillary pressure and dispersivities have been shown in Table 2 for three solutions. The maximum element growth rate used was 1.1, while the maximum and minimum sizes of the elements were 0.48 cm and 0.00094 cm, respectively. To enhance the convergence of the numerical model, the mesh was refined in the vicinity of the injection port, with a maximum element size of 0.11 cm. The finite element solver used was MUMPS (multifrontal massively parallel sparse direct solver) within COMSOL Multiphysics. For the time-stepping approach, a backward differentiation formula (BDF) was employed, along with the free time-stepping option, enabling flexible time steps to meet the specified tolerance. The tolerance factor used was 0.1. The boundary conditions for 2D tank, the constant injection rate of 2 mL/min and injection concentration of each component for the injection port and constant pressure for the lateral and upper boundaries were considered (Fig. 2).

2.5. Image analysis

Image analysis was used to track changes in the two-phase flow inside the porous medium over time and estimate DNAPL saturation. To capture high-quality images, a Nikon® D810 was used in a dark room, illuminated by two 300 W (Broncolor®) floodlights. To reduce reflections and optimize contrast, black and white reflectors were placed at precise locations in the laboratory. A grayscale calibration card was positioned on the front surface of the 2D tank to regulate the light density during image analysis. Using the 8-grayscale levels the lighting variances were modified. To minimize the impact of wall shading on the

Table 2
Relative permeability and capillary pressure parameters used in modeling and mean average error of experimental and numerical data for 2D tank.

System	Solution	k_{rw}^{max} (−)	k_{rnw}^{max} (−)	ε_w (−)	ε_{nw} (−)	λ	$p_{th}(Pa)$	S_{wr} (−)	S_{nwr} (−)	$\propto_L$ (cm)	$\propto_T$ (cm)	MAE (Mean Absolute Error)
	Mixture	0.5	0.7	2.5	3			0.12	0.3			0.102
Unconfined	NaI	0.5	0.7	2.5	3	2	500	0.12	0.32	0.1	0.001	0.103
	Xanthan	0.8	0.55	2.3	3			0.12	0.48			0.084
Confined multilayer	Mixture	0.7	0.6	2.3	3.2			0.08	0.22			0.018

Boundaries 1-3: P= P_0+(0.2-z (m))×16600 Pa

C_i=0

Boundaries 4-5: No-flow boundary

C_i=0

Fixed injection rate:

2 mL/min

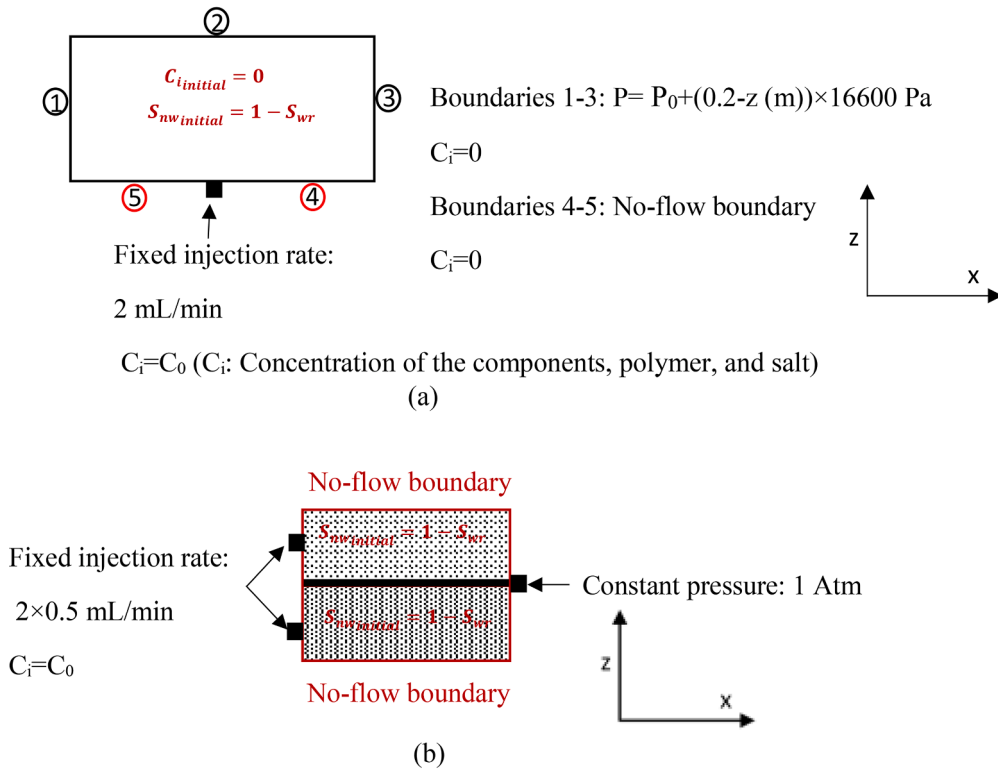C_i=C_0 (C_i: Concentration of the components, polymer, and salt)

(a)

(b)

Fig. 2. Schematic of boundary and initial conditions for numerical simulations in 2D tank. (a) unconfined single layer 2D tank, (b) confined two-layer 2D tank.

phases' saturation calculation, the size of the area of interest (AOI) was chosen to be almost the same as the lateral surface of the tank glass (Alamooti et al., 2022; Colombano et al., 2021; Philippe et al., 2020). The optical density of reflected light O_d, is considered as (Flores et al., 2011)

$$O_d = -\log(\rho_t) \tag{13}$$

$$\rho_t = \frac{I_r}{I_0} \tag{14}$$

where optical density of reflected light is denoted as O_d(-), and the ratio of reflected luminous intensity I_r(-) to the initial luminous intensity I_0(-) is represented as ρ_t(-).

Next, optical densities were measured at four points: points where the porous medium was fully saturated with water and DNAPL, as well as points with known residual saturations of DNAPL and water. A linear calibration curve was used to correlate the optical densities with DNAPL saturation (Alamooti et al., 2022; Colombano et al., 2020). The average DNAPL saturation for the entire area of interest (AOI) was determined by summing the individual saturations for each pixel, which were

obtained from the optical density measurements. The calculated saturation was then compared to those obtained through mass balance calibration.

3. Results and discussion

3.1. Rheological behavior in bulk and porous media

Fig. 3 displays the rheological behaviour of xanthan solution with and without NaI, along with the fitted Carreau fluid model (Carreau, 1972) expressed as:

$$\mu = \mu_{inf} + (\mu_0 - \mu_{inf})(1 + (\chi\dot{\gamma})^2)^{\frac{l-1}{2}} \tag{15}$$

where, μ_0 and μ_{inf} represent the viscosities (Pa s) at zero and infinite shear rate respectively, χ denotes the relaxation time (s), and l (-) indicates the power index. The parameters of Carreau model for xanthan solutions in the presence and absence of NaI are shown in Table 3. As it can be seen the results from Carreau model is properly fit with experimental results.

The experimental results show that xanthan exhibit a shear thinning behavior which is preserved in the presence of NaI while the viscosity of
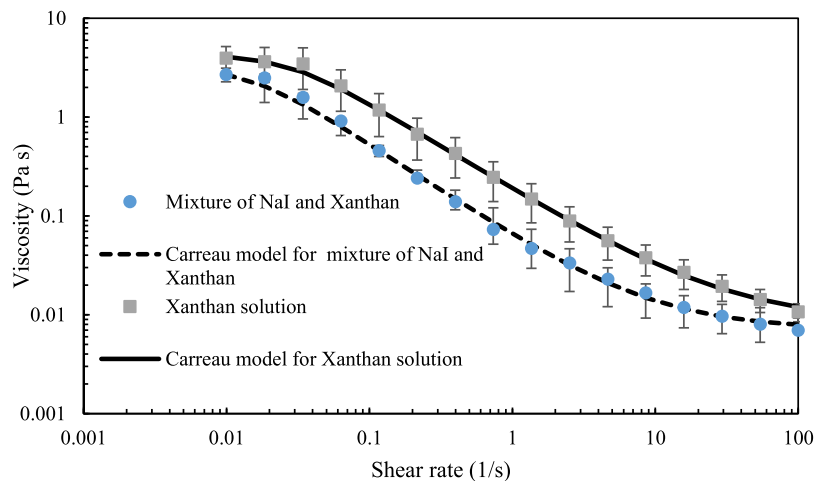
Fig. 3. Rheological behavior of xanthan solution at a concentration of 800 mg/L and mixture of xanthan and NaI with xanthan concentration of 590 mg/L and NaI concentration of 960.11 g/L as well as Carreau models fitted on experimental data. Experiments have been triplicated and error bars are calculated by determining the mean (average) of the data points and the standard deviation.

Table 3
Parameters of Carreau model for pure xanthan and mixture of xanthan and NaI.

Solution	μ_{inf} (Pa s)	μ_0 (Pa s)	χ (s)	l (−)	R^2
Xanthan solution	0.0087	4.310	36.755	0.1237	0.988
Mixture of xanthan and NaI	0.0072	3.214	67.330	0.0515	0.988

the solution is reduced (Najjari et al., 2016). This can be justified by the lower concentration of xanthan in the mixture due to the increase in volume of solution by dissolution of NaI. Also, xanthan as a long-chain polysaccharide contains negatively charged chemical groups, such as acetyl and pyruvate groups. The electrostatic repulsion between these negative charges cause the xanthan molecules to extend and form a coiled shape due to electrostatic repulsion (Carrington et al., 1996). However, when salt ions are present, they reduce the electrostatic repulsion and cause the xanthan molecule to collapse into a more compact and rod-like shape. As a result, the negatively charged groups are positioned closer to the molecule's backbone, which leads to a decrease in its hydrodynamic volume (Higiro et al., 2007; Rochefort and Middleman, 2000). The lower the hydrodynamic volume the easier xanthan molecules can move in the solution; resulting in a reduction in viscosity. As a result the viscosity of mixture of NaI and xanthan is lower than the one for pure xanthan solution. This difference is most pronounced in the intermediate range of shear rates, where an average reduction in viscosity by a factor of 2.6 is observed. However, at very high or low shear rates, the viscosity decrease is approximately by a factor of 1.5.

Single–phase flow 1D column experiments were performed to assess the rheological behavior of xanthan solutions with and without NaI in porous media. The shear rate in porous media can be expressed as (Darby et al., 2017):

$$\dot{\gamma} = \sqrt{\frac{2}{\phi k}} \alpha u \tag{16}$$

The shift factor, α (-), is associated with the properties of the porous medium and the rheological properties of the fluid at bulk (Chauveteau and Zaitoun, 1981).

The apparent shear rate is obtained using the apparent viscosity derived from the column experiment, after rearranging the Carreau fluid model based on its determined parameters. Then the apparent shear rate is plotted against the Darcy velocity $\frac{u}{\sqrt{\phi k}}$. The slope of the fitted linear curve passing through the origin was then found and considered as the

shift parameter (Zamani et al., 2015). The viscosity data obtained from the porous media experiments compared with those at bulk are shown in Fig. 4.

The shift parameter is 0.6 and 0.45 for xanthan solution and the mixture of xanthan and NaI, showing that the apparent viscosity in our porous medium is globally higher than that in bulk fluid. The flow of polymers in porous media can be understood by looking at the pore and throat structure as a sequence of expanding and contracting channels. The polymer molecules deform as they pass through the contractions, causing an increase in resistance to flow (Holmberg et al., 2002). When NaI is present in the polymer solution can lead to a decrease in electrostatic repulsion, causing the xanthan molecule to condense into a compact, rod-like structure. As a result, polymer molecules align along the flow direction. This leads to a smaller shift factor compared to that of a pure xanthan solution. The influence of the depleted layer near the pore wall is relatively insignificant due to the high permeability of the porous media (Chauveteau and Zaitoun, 1981).

3.2. Two-phase flow columns experiments

Two-phase flow column experiments were conducted to assess the efficiency of injecting various solutions for displacing DNAPL in a closed horizontal system. The termination criterion for the experiments was reached when no further DNAPL was observed in the effluents. The 1D column results shown in Fig. 5a indicate that the recovery efficiency $\left(\frac{\text{volume of DNAPL recovered}}{\text{initial volume of DNAPL in sand}} \right)$ as a function of PV for xanthan solutions, with or without NaI, are nearly identical, whereas the recovery efficiency is slightly higher for pure xanthan solution due to its higher viscosity compared to the mixture of xanthan and NaI. The recovery efficiency for pure NaI solution is lower, at around 0.74, as its viscosity is significantly lower than that of the polymer solutions. During the injection of various solutions, the capillary number was calculated using the following equation to evaluate their effectiveness in displacing DNAPL (Chatzis and Morrow, 1984):

$$N_{ca} = \frac{k\nabla p}{\sigma} \tag{17}$$

where σ (N/m) is the interfacial tension (IFT) between the DNAPL and the different solutions. The IFT between DNAPL and a mixture of xanthan and NaI, pure NaI solution and xanthan solution were measured as 10.87 ± 0.05, 10.14 ± 0.05, and 21.5 ± 0.05 mN/m, respectively. The capillary number plots (Fig. 5b) show that the capillary number at the end of the experiment as a function of PV is almost identical for injection
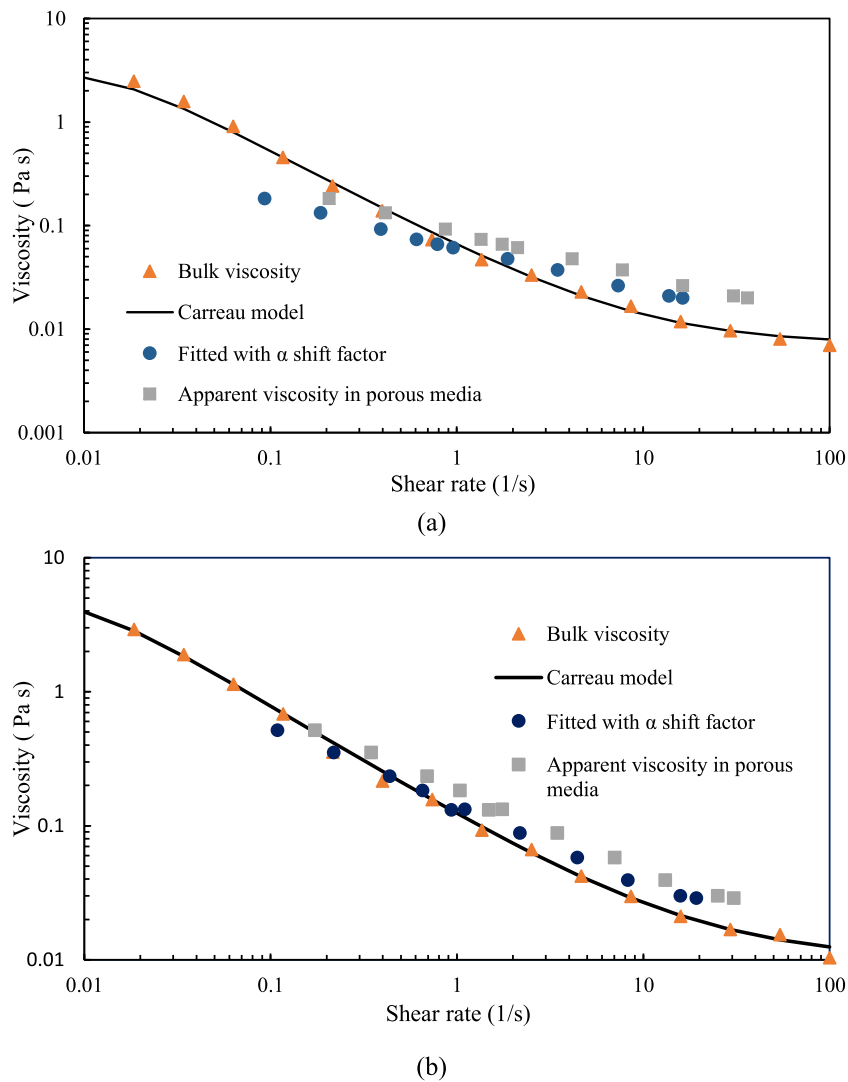
Fig. 4. Apparent viscosity compared with those obtained from rheometer. (a) mixture of xanthan and NaI, (b) pure xanthan solution.
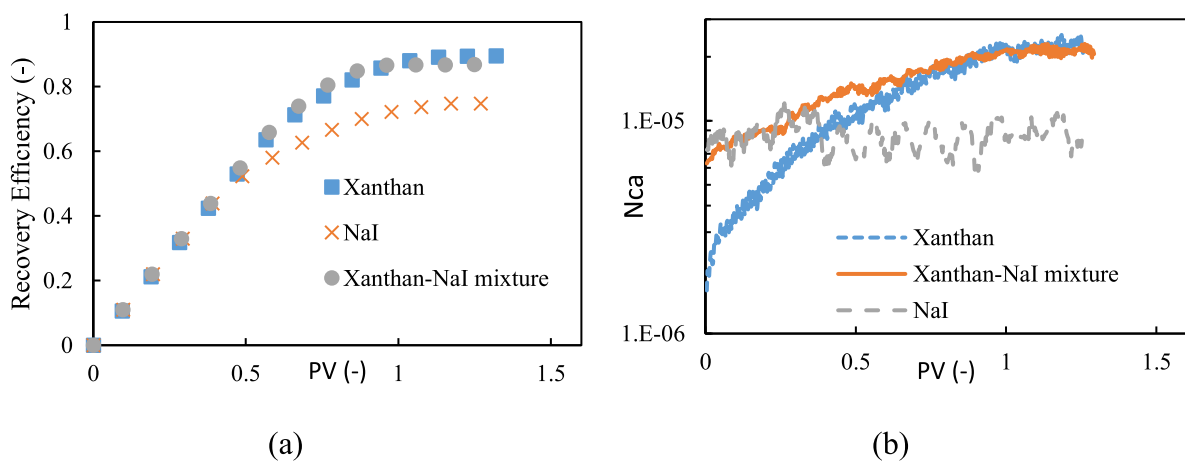

Fig. 5. Performance of injection of different solutions. (a) Recovery efficiency, (b) Capillary number versus injected PV.

of xanthan and the mixture of xanthan and NaI. Moreover, it is higher compared to the pure NaI solution, which is in line with the recovery efficiency results. The oscillations in capillary number plot of pure NaI solution is attributed to the pressure fluctuations caused by peristaltic pump which is directly detected by pressure sensors as there is no polymer inside the solution to dampen it.

3.3. Two-dimensional flow (unconfined 2D tank)

The role of gravity cannot be accurately observed in a horizontal 1D column system, as the thickness of the polluted zone (diameter of the column) is too small, and the system is closed, prohibiting vertical movement. The 2D experiments were performed to evaluate the efficiency of the injection of the three aforementioned solutions on the displacement of DNAPL layer in an unconfined system were the gravity can significantly influence the propagation of the invaded fluid. The solutions containing a colorant were individually injected into the tank saturated with DNAPL in presence of residual water following the steps mentioned in Section 2.1. Fig. 6 shows the propagation of different solutions at the end of the experiments. The interface between the invading solution and DNAPL is depicted by the white dashed lines. In the case of a mixture of xanthan and NaI (Fig. 6a), two white lines are present, representing the interface for the fully and partially displaced zones.

When NaI is present in the polymer solution, a lateral displacement can be observed (Fig. 6a); however, in the absence of xanthan in NaI solution the displacement is less effective and there are areas where the black color of the DNAPL remains more prominent (Fig. 6b). Injection of pure xanthan results in a main vertical movement (Fig. 6c). The evolution of the front propagation of the injected fluid through the contaminated zone is shown in Fig. 7.

The observations in Fig. 7 indicate that in cases where NaI is present in the solution, the solution propagations exhibit similar radial/lateral patterns through the contaminated zone. In contrast, when using pure xanthan, the lateral propagation becomes limited over time, and the movement is predominantly vertical. For the case of injection of the mixture, a fully displaced zone and a transition zone can be observed (Fig. 6a). The recovery efficiency curves for injection of each solution are shown in Fig. 8, which exhibit values around 0.46, 0.24, and 0.09 at the end of the displacement for the mixture of xanthan and NaI, pure NaI, and xanthan solutions, respectively. The propagation of the invading solution in the contaminated zone can be described through aspect ratio values (see Fig. 6) which is defined as the ratio of the lateral radius R_L to vertical radius R_V (Davarzani et al., 2021). When both transition and fully displaced zones are present in the system, for the determination of the aspect ratio, R_L and R_V correspond to the radii of the fully displaced zone. The aspect ratios are around 1.21, 1 and 0.38 for the mixture of xanthan and NaI, pure NaI, and xanthan solutions, respectively. The low recovery efficiency even when the aspect ratio favors the displacement of DNAPL is attributed to the unconfined nature of the system which is close to the real polluted site (Alamooti et al.,

2022).

Numerical modeling was performed to have a better understanding of the underlying physics behind the experiments. Using the data obtained from 1D column experiments (directly and indirectly through inverse modeling), the displacement of DNAPL through the 2D tank was simulated. Fig. 9 shows the comparison between the numerical and experimental results after image analysis. The recovery efficiency curves obtained from the experiments and modeling are shown in Fig. 10. These results demonstrate that the numerical modeling can properly predict the experimental consequences, where the mean absolute error between the numerical and experimental results is around 0.1. Also, the dynamic of propagation of the invading phases for different solution during the experiments has been appropriately captured by simulation results which are shown in Fig. 10.

3.4. Gravity number analysis

The displacement of DNAPL through the 2D system is influenced by gravity, viscous and capillary forces. The gravity number given by Eq. (1) can show how effectively gravity and viscous forces are playing a role on the propagation of the injected fluids in the contaminated zone. Using the developed numerical model that has properly captured experimental consequences, an analysis was performed to evaluate the changes in aspect ratio of the invading fluid versus the changes in gravity number (Cochennec et al., 2022). To investigate this, a range of injection velocities and different densities of the invading phase were considered. The corresponding viscosity was determined by establishing a relationship between the apparent viscosity of the invading phase and the pressure gradient obtained from column experiments. Fig. 11 displays the results, showing that for gravity numbers less than -0.25, a very slight increase in aspect ratio is observed, indicating a preference for vertical migration of the invading phase when the density of the invading phase is lower than that of the DNAPL. Then, a sharp increase in aspect ratio for the gravity numbers between -0.25 and 0.25 can be observed, demonstrating a favorable displacement where a radial displacement can be observed. For higher gravity numbers, the slope of increase in aspect ratio decreases as the denser invading phase reaches the lateral boundaries and its lateral movement stops (Cochennec et al., 2022). The results showing that an increase in the gravity number due to densification of the polymer solution can hinder vertical movement of the invading fluid, but may result in an underriden flow where the invading fluid flows below the contaminated zone.

3.5. DNAPL displacement in confined two-layer system by densified polymer solution

Multiphase flow experiments were conducted in a two-layer 2D system, following the procedures outlined in Section 2.2. Xanthan solutions, both with and without NaI, were injected individually through contaminated layers to displace DNAPL. In Fig. 12, the propagation of polymer solutions in DNAPL-saturated layers is illustrated at different
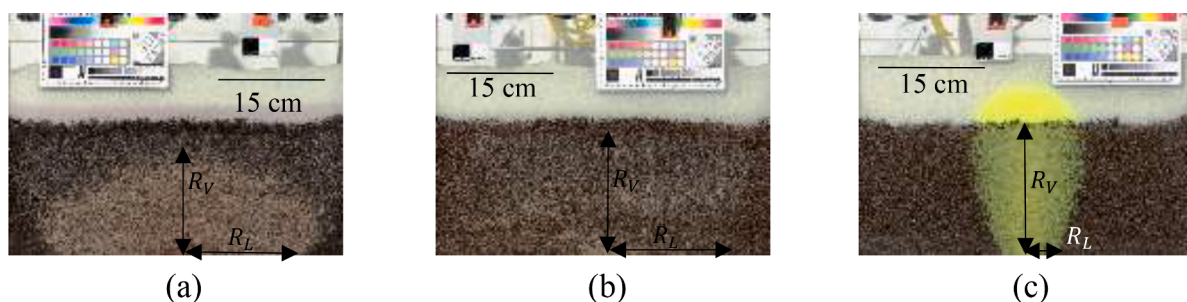

Fig. 6. Comparison of the propagation of three solutions at the end of injection through the contaminated zone, DNAPL appears black and displaced zone is bright. (a) Mixture of xanthan and NaI, (b) pure NaI brine, and (c) xanthan solution.
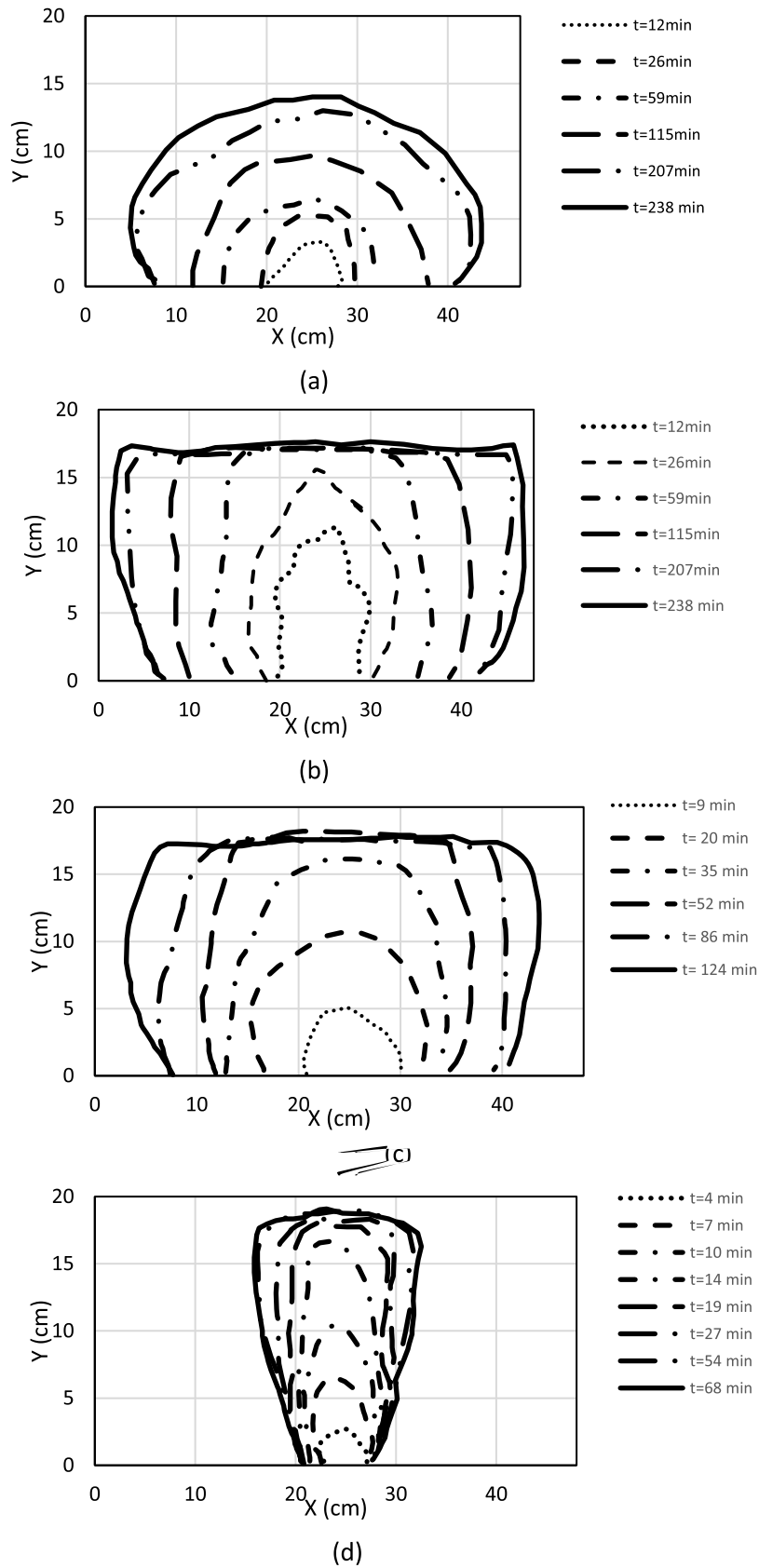
Fig. 7. Dynamic of propagation of the fluids during injection through the DNAPL contaminated zone. (a) fully displaced zone for injection of mixture of xanthan and NaI, (b) transition displaced zone for injection of mixture of xanthan and NaI, (c) displaced zone for injection of NaI brine solution, and (d) displaced zone for injection of xanthan solution.
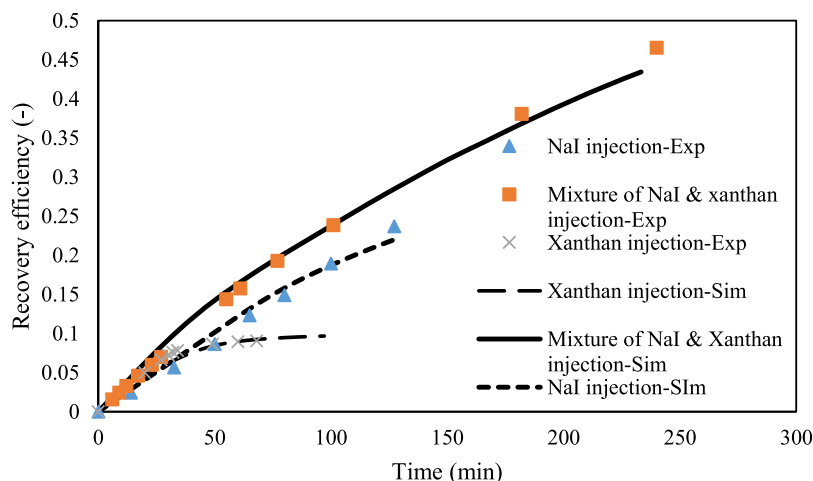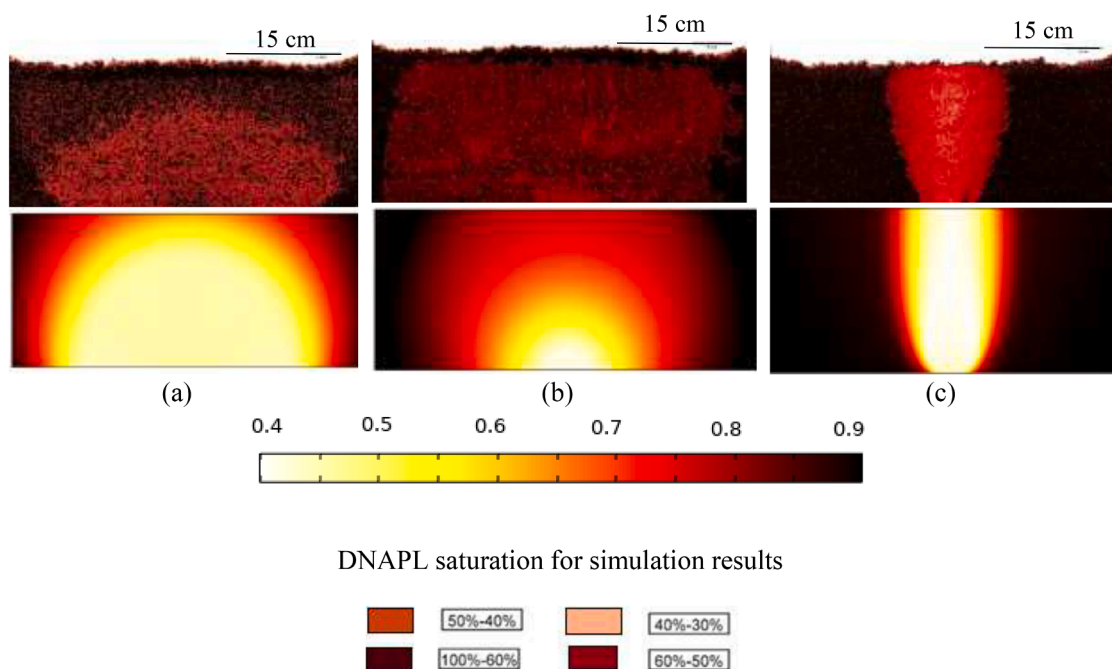
Fig. 8. Comparison of recovery factor obtained from experiments and simulations for injection of different solutions including mixture of xanthan and NaI solution, pure NaI solution, and xanthan solution.

Fig. 9. Comparison between the numerical and experimental results at the end of the displacement of DNAPL by different solutions, the first row images are extracted from the image analysis of experiments and the second row images are from the simulation. (a) Mixture of NaI and xanthan (b) pure NaI, (c) and pure xanthan.

injected PVs. The experimental results indicate similar DNAPL displacement for both non-densified and densified polymer solutions. This similarity can be attributed to the role of the closed upper boundary, which hinders the vertical movement of the non-densified polymer solution. Additionally, irrespective of the density of invading polymer solutions, a density-overridden flow is observed.

In the case of xanthan-NaI, this overridden flow can be explained by the mixing of the invading densified solution and residual water in the system, resulting in a reduction in the density of the flowing aqueous phase. Consequently, a preference for flowing on the top of the layers is observed. The permeability contrast influences the flow as DNAPL is initially drained from the higher permeable layer. The results for the distribution of xanthan-NaI and DNAPL by numerical simulation are also

depicted in the third line of Fig. 12, capturing the experimental consequences, including the density-overridden flow.

Fig. 13 illustrates the recovery curves obtained from 2D experiments for both polymer solutions, indicating a higher recovery efficiency for pure xanthan solution. This finding is consistent with 1D column results and is attributed to its slightly higher viscosity. Additionally, the recovery efficiency curve obtained from simulation for the xanthan-NaI case is demonstrated in Fig. 13, showing good consistency with the experimental results.
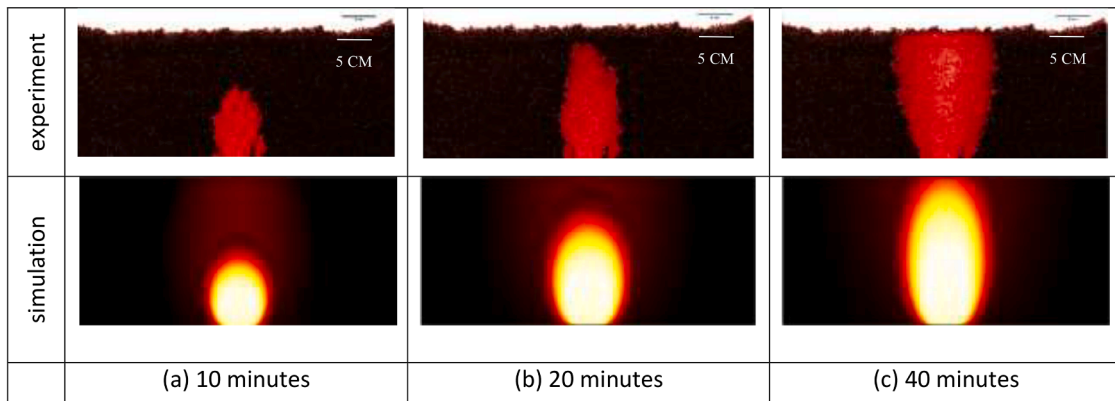
To assess the impact of permeability contrast on the displacement of DNAPL, we conducted numerical simulations by varying the permeability ratios of two layers. These simulations were compared with experimental results, where the DNAPL in the bottom layer reached half
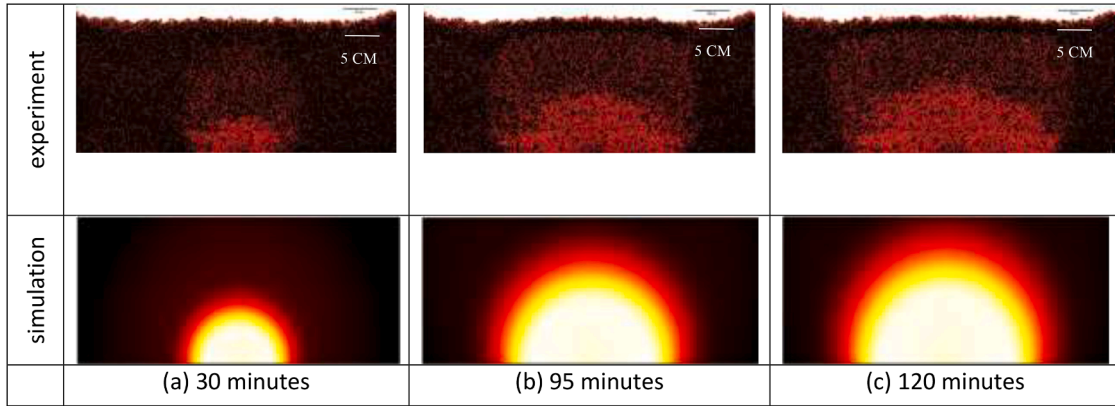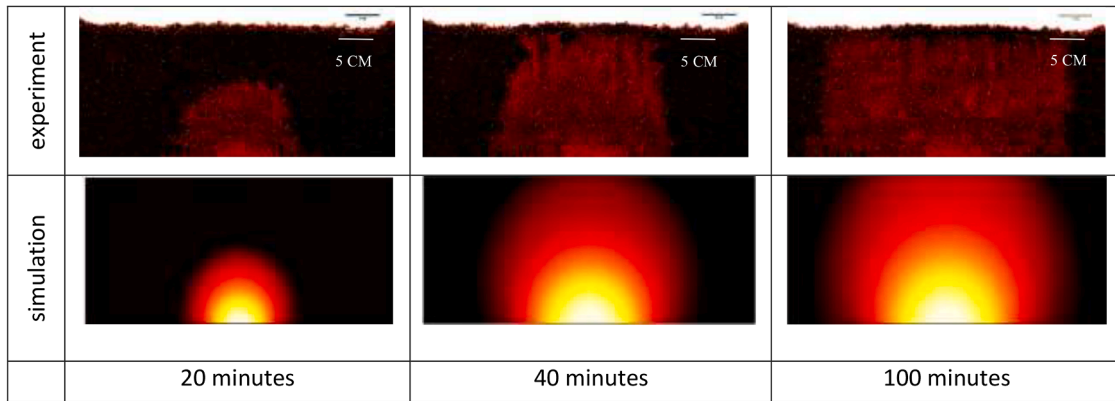
Fig. 10. Comparison of the propagation of invading solutions and DNAPL in 2D tank at different times, (a) mixture of xanthan and NaI solution, (b) pure NaI solution, and (c) pure xanthan solution.
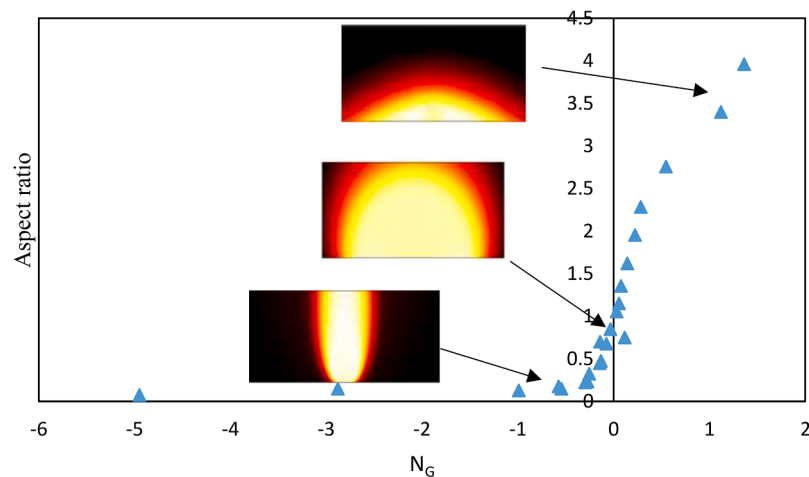
Fig. 11. Changes in aspect ratio of invaded fluid based on gravity number using numerical simulations in 2D tank domain.
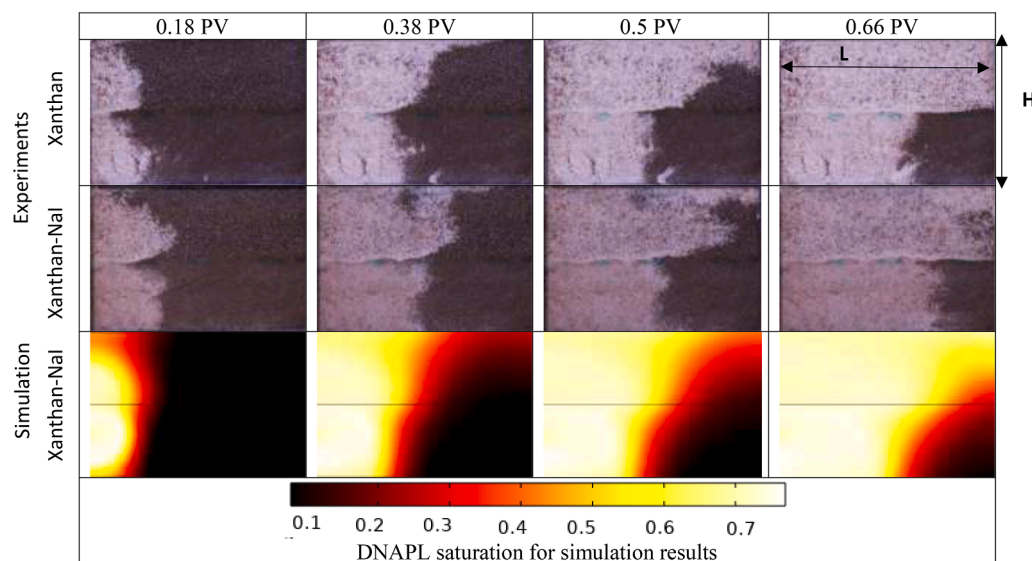

Fig. 12. DNAPL displacement in a 2D multilayer system by injection of pure xanthan solution (first row), mixture of xanthan-NaI (second row) and numerical simulation for xanthan-NaI (third row) at different pore volumes of injected fluids.

of the horizontal axis. The front shape from simulation results were specifically extracted from the middle of the transition zone and compared to the experimental data. Fig. 14 illustrates the propagation of fronts for various permeability ratios (K_{upper}/K_{lower}) in a 2D system with a vertical axis of relative height (y/H) and a horizontal axis of relative length (x/L). The results indicate that increasing the values of K_{upper}/K_{lower} leads to a rapid breakthrough, where both permeability contrast and density-driven flow synergistically contribute to the flow in the upper layer. Simultaneously, a significant amount of DNAPL can remain untouched in the lower layer. Conversely, lower values of K_{upper}/K_{lower} demonstrate an opposing influence of density difference and permeability contrast on the flow. Even at a K_{upper}/K_{lower} ratio equal to 1/10, the front in the bottom layer remains considerably distant from the recovery point. Notably, when there is no permeability contrast between the layers, a slightly inclined front is observed.

Another crucial factor influencing the front shape in a multilayer system is the ratio of the length to height of the tank (L/H). In this context, the length of the system was varied in numerical simulations to cover the range of L/H from 0.5 to 20. Similar to the previous case, these simulations were then compared with experimental results where the DNAPL in the bottom layer reached half of the horizontal axis.

The results depicted in Fig. 15 reveal that as the length of the system increases to achieve higher L/H ratios, the influence of density difference on the flow diminishes. A steep front, without a noticeable preference for flow on the top, becomes apparent. Conversely, for lower L/H values, density-driven flow can lead to a rapid breakthrough, with a front inclined toward the recovery point and propagation occurring in the upper parts of the system.

3.6. Sensitivity analysis

The injection of NaI-xanthan mixture into the unconfined two-dimensional aquifer sandbox was selected as the experimental setup to explore the impact of various numerical modeling parameters on the shape of the fully displaced zone's front at the 115th min. The optimal front shape for each parameter was compared with simulations employing higher or lower values of that specific parameter, while keeping other numerical modeling parameters constant at the fitted values detailed in Table 2. The results, depicted in Fig. 16, highlight that among the relative permeability terms, the saturation exponents exert a more pronounced influence on the front shape than the maximum relative permeability values. Regarding capillary pressure terms, a lower
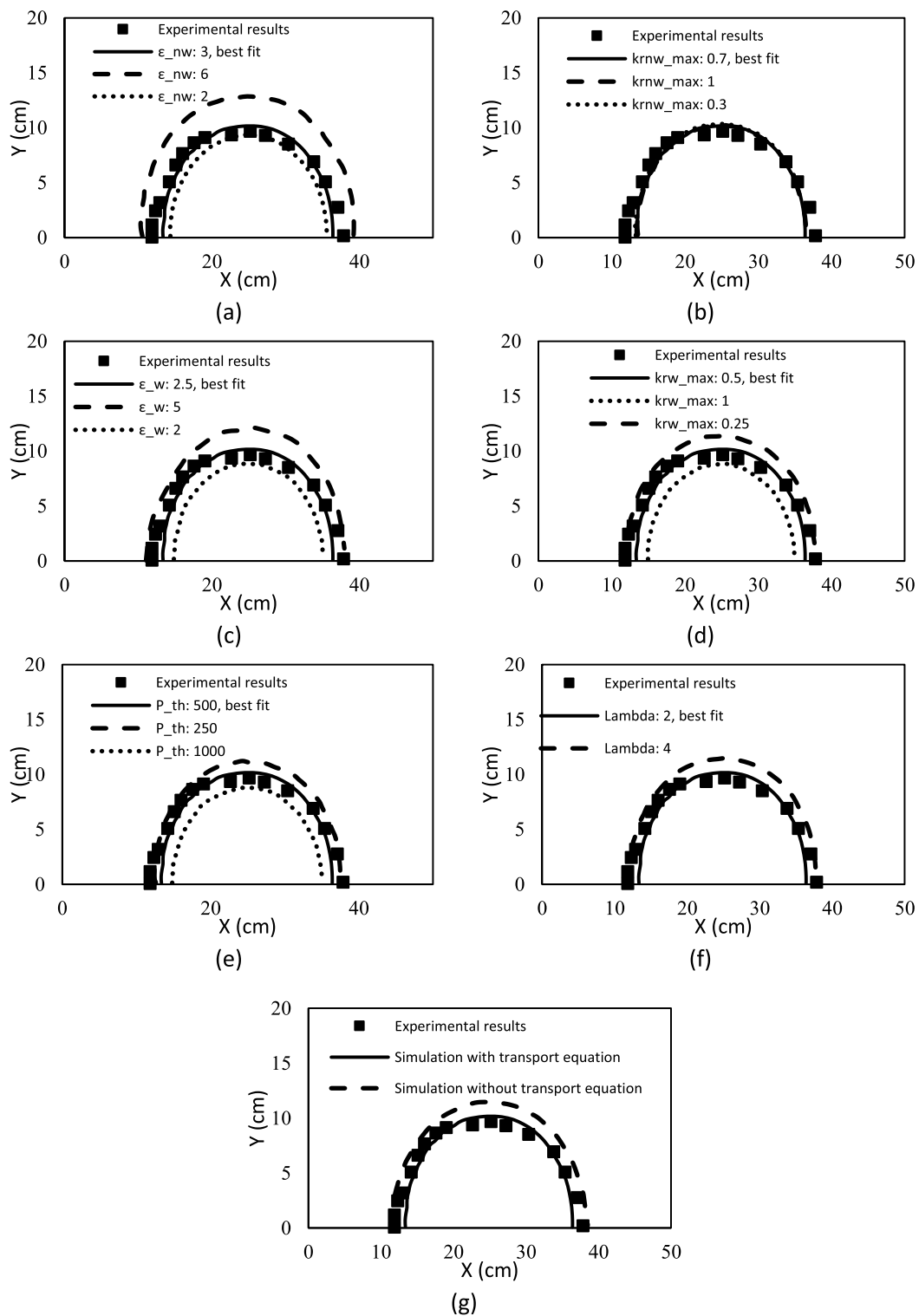
Fig. 13. Recovery efficiency curve for experiments of injection of pure xanthan and xanthan-NaI mixture into multilayer system and results from numerical simulation for xanthan-NaI mixture injection.
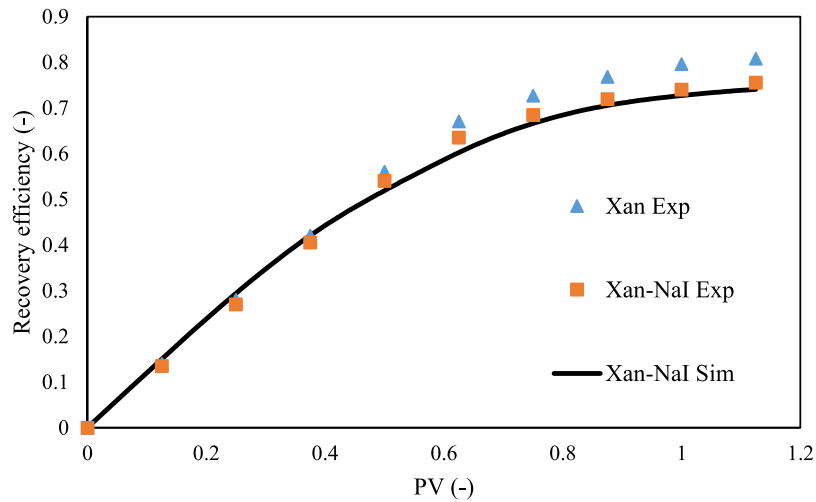
Fig. 14. Effect of permeability contrast on propagation of invading xanthan-NaI solution in DNAPL saturated two-layer system.
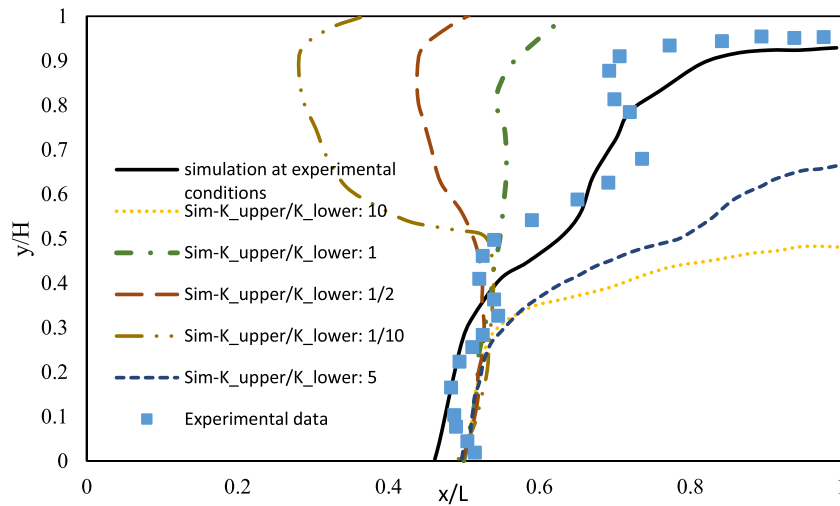

Fig. 15. Effect of L/H ratios on propagation of invading xanthan-NaI solution in DNAPL saturated two-layer system.
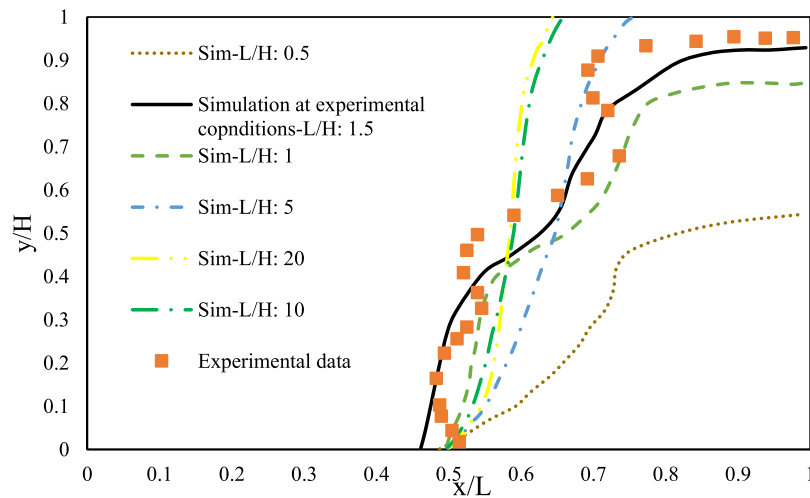

Fig. 16. Sensitivity analysis of numerical simulation parameters compared with selected experiment. (a) non wetting phase relative permeability saturation exponent, (b) non wetting phase maximum relative permeability, (c) wetting phase relative permeability saturation exponent, (d) wetting phase maximum relative permeability, (e) threshold pressure, (f) pore size distribution, and (g) transport equation.

threshold pressure and a higher pore size distribution lead to a more invaded front compared to the experimental results. Similarly, excluding the transport equation in numerical simulations results in a larger (expanded) front.

4. Conclusions

A set of experiments including rheological measurement in the bulk fluid and in porous media, as well as two-phase flow in 1D columns and 2D tanks was performed to evaluate the efficiency of the injection of densified NaI solutions with and without xanthan and a pure xanthan solution on the displacement of DNAPL. A numerical simulation consistent with the experimental consequences was also performed to analyze the role of gravity and viscous forces on the propagation of the polymer solution (with different degrees of densification) in 2D systems.

Rheological measurements showed that the addition of NaI as a densifier did not affect the shear-thinning behavior of xanthan, but the presence of ions reduced the viscosity by a factor of 2.6 for intermediate range of shear rate. The shift factor for apparent viscosity was less than unity, indicating a deformation of polymer molecules and an increased flow resistance due to contractions and expansions in porous media. Confined column experiments revealed similar recovery efficiencies of around 0.89 for xanthan solutions regardless of density, while the pure brine solution had a lower recovery efficiency of around 0.74, consistent with capillary number analysis.

In open 2D tank experiments, gravity and viscous forces cooperatively influenced DNAPL displacement efficiency. Pure xanthan solution injection showed vertical displacement with an aspect ratio of 0.38 and recovery efficiency of 0.09, while densified polymer solution invaded the contaminated zone radially with an aspect ratio of 1.21 with a recovery efficiency of 0.46. Pure brine solution reached most of the contaminated zone, but the black color of the DNAPL remained more prominent in displaced zone resulted in recovery efficiency of 0.24. Numerical simulations indicated that a gravity number close to zero is needed to achieve an aspect ratio around unity and avoid density-driven flow issues.

Injection of both densified and non-densified polymer solutions resulted in a preferential flow on top of multilayer system. In the case of xanthan-NaI, this overridden flow can be explained by the mixing of the invading densified solution and residual water in the system, resulting in a reduction in the density of the flowing aqueous phase. The numerical simulation results indicate that increasing the values of K_{upper}/K_{lower} leads to a rapid breakthrough, where both permeability contrast and density-driven flow synergistically contribute to the flow in the upper layer.

Note

A patent application has been filed with the reference: FR 2305516.

CRediT authorship contribution statement

Amir Alamooti: Conceptualization, Formal analysis, Methodology, Software, Visualization, Writing – original draft. **Stéfan Colombano:** Conceptualization, Funding acquisition, Project administration, Supervision, Writing – review & editing. **Dorian Davarzani:** Supervision, Writing – review & editing. **Fabien Lion:** Visualization. **Azita Ahmadi-Sénichault:** Supervision, Validation, Writing – review & editing.

Declaration of competing interest

The authors declare that they have no known competing financial interests or personal relationships that could have appeared to influence the work reported in this paper.

Data availability

The data that has been used is confidential.

References

Alamooti, A., Colombano, S., Glabe, Z.A., Lion, F., Davarzani, D., Ahmadi-Sénichault, A., 2023. Remediation of multilayer soils contaminated by heavy chlorinated solvents using biopolymer-surfactant mixtures: two-dimensional flow experiments and simulations. Water Res. 243, 120305 https://doi.org/10.1016/j.watres.2023.120305.

Alamooti, A., Colombano, S., Omirbekov, S., Ahmadi, A., Lion, F., Davarzani, H., 2022. Influence of the injection of densified polymer suspension on the efficiency of DNAPL displacement in contaminated saturated soils. J. Hazard. Mater. 440, 129702 https://doi.org/10.1016/j.jhazmat.2022.129702.

Alamooti, A.H., Azizi, Q., Davarzani, D., 2020. Direct numerical simulation of trapped-phase recirculation at low capillary number. Adv. Water Resour. 145, 103717 https://doi.org/10.1016/j.advwatres.2020.103717.

Alamooti, A., Colombano, S., Shoker, A., Ahmadi-Sénichault, A., Lion, F., Cazaux, D., Marion, C., Lagron, J., Sawadogo, I., Davarzani, D., 2024. Enhancing remediation of residual DNAPL in multilayer aquifers: Post-injection of alcohol-surfactant-polymer mixtures. Science of The Total Environment 170680. https://doi.org/10.1016/j.scitotenv.2024.170680.

Anderson, D.M., McLaughlin, R.M., Miller, C.T., 2003. The averaging of gravity currents in porous media. Phys. Fluids 15, 2810–2829. https://doi.org/10.1063/1.1600733.

Auset, M., Keller, A.A., 2004. Pore-scale processes that control dispersion of colloids in saturated porous media. Water Resour. Res. 40 https://doi.org/10.1029/2003WR002800.

Bear, J., 2013. Dynamics of Fluids in Porous Media. Courier Corporation.

Bouzid, I., Fatin-Rouge, N., 2022. Assessment of shear-thinning fluids and strategies for enhanced in situ removal of heavy chlorinated compounds-DNAPLs in an anisotropic aquifer. J. Hazard. Mater. 432, 128703 https://doi.org/10.1016/j.jhazmat.2022.128703.

Brooks, R.H., Corey, A.T., 1964. Hydraulic properties of porous media and their relation to drainage design. Trans. ASAE 7, 26–28.

Carreau, P.J., 1972. Rheological equations from molecular network theories. Trans. Soc. Rheol. 16, 99–127. https://doi.org/10.1122/1.549276.

Carrington, S., Odell, J., Fisher, L., Mitchell, J., Hartley, L., 1996. Polyelectrolyte behaviour of dilute xanthan solutions: salt effects on extensional rheology. Polymer 37, 2871–2875. https://doi.org/10.1016/0032-3861(96)87653-1 (Guildf).

Chatzis, I., Morrow, N.R., 1984. Correlation of capillary number relationships for sandstone. Soc. Pet. Eng. J. 24, 555–562. https://doi.org/10.2118/10114-PA.

Chauveteau, G., Zaitoun, A., 1981. Basic rheological behavior of xanthan polysaccharide solutions in porous media: effects of pore size and polymer concentration. In: Proceedings of the First European Symposium on Enhanced Oil Recovery, Bournemouth, England. Richardson, TX. Society of Petroleum Engineers, pp. 197–212.

Ciriello, V., Di Federico, V., Archetti, R., Longo, S., 2013. Effect of variable permeability on the propagation of thin gravity currents in porous media. Int. J. Non Linear Mech. 57, 168–175. https://doi.org/10.1016/j.ijnonlinmec.2013.07.003.

Cochennec, M., Davarzani, H., Davit, Y., Colombano, S., Ignatiadis, I., Masselot, G., Quintard, M., 2022. Impact of gravity and inertia on stable displacements of DNAPL in highly permeable porous media. Adv. Water Resour. 162, 104139 https://doi.org/10.1016/j.advwatres.2022.104139.

Colombano, S., Davarzani, H., van Hullebusch, E.D., Huguenot, D., Guyonnet, D., Deparis, J., Ignatiadis, I., 2020. Thermal and chemical enhanced recovery of heavy chlorinated organic compounds in saturated porous media: 1D cell drainage-imbibition experiments. Sci. Total Environ. 706, 135758 https://doi.org/10.1016/j.scitotenv.2019.135758.

Colombano, S., Davarzani, H., van Hullebusch, E.D., Huguenot, D., Guyonnet, D., Deparis, J., Lion, F., Ignatiadis, I., 2021. Comparison of thermal and chemical enhanced recovery of DNAPL in saturated porous media: 2D tank pumping experiments and two-phase flow modelling. Sci. Total Environ. 760, 143958 https://doi.org/10.1016/j.scitotenv.2020.143958.

Damrongsiri, S., Tongcumpou, C., Sabatini, D.A., 2013. Partition behavior of surfactants, butanol, and salt during application of density-modified displacement of dense non-aqueous phase liquids. J. Hazard. Mater. 248, 261–267.

Darby, Ronald, Darby, Ron, Chhabra, R.P., 2017. Chemical Engineering Fluid mechanics, Revised and Expanded. CRC Press. https://doi.org/10.1201/9781315274492.

Davarzani, H., Aranda, R., Colombano, S., Laurent, F., Bertin, H., 2021. Experimental study of foam propagation and stability in highly permeable porous media under lateral water flow: diverting groundwater for application to soil remediation. J. Contam. Hydrol. 243, 103917 https://doi.org/10.1016/J.JCONHYD.2021.103917.

Di Federico, V., Longo, S., Chiapponi, L., Archetti, R., Ciriello, V., 2014. Radial gravity currents in vertically graded porous media: theory and experiments for Newtonian and power-law fluids. Adv. Water Resour. 70, 65–76. https://doi.org/10.1016/j.advwatres.2014.04.015.

Di Federico, V., Longo, S., King, S.E., Chiapponi, L., Petrolo, D., Ciriello, V., 2017. Gravity-driven flow of Herschel–Bulkley fluid in a fracture and in a 2D porous medium. J. Fluid Mech. 821, 59–84.

Du, H., Zhao, Z., Cheng, H., Yan, J., He, Q., 2023. Modeling density-driven flow in porous media by physics-informed neural networks for CO2 sequestration. Comput. Geotech. 159, 105433 https://doi.org/10.1016/j.compgeo.2023.105433.

Fitzhenry, E., Martel, R., Robert, T., 2022. Foam injection for enhanced recovery of diesel fuel in soils: sand column tests monitored by CT scan imagery. J. Hazard. Mater. 434, 128777.

Flores, G., Katsumi, T., Inui, T., Kamon, M., 2011. A simplified image analysis method to study LNAPL migration in porous media. Soils Found. 51, 835–847.

Giese, S.W., Powers, S.E., 2002. Using polymer solutions to enhance recovery of mobile coal tar and creosote DNAPLs. J. Contam. Hydrol. 58, 147–167. https://doi.org/10.1016/S0169-7722(02)00009-8.

Grubb, D.G., Sitar, N., 1999. Mobilization of trichloroethene (TCE) during ethanol flooding in uniform and layered sand packs under confined conditions. Water Resour. Res. 35, 3275–3289. https://doi.org/10.1029/1999WR900222.

Higiro, J., Herald, T.J., Alavi, S., Bean, S., 2007. Rheological study of xanthan and locust bean gum interaction in dilute solution: effect of salt. Food Res. Int. 40, 435–447. https://doi.org/10.1016/J.FOODRES.2006.02.002.

Holmberg, K., Jönsson, B., Kronberg, B., Lindman, B., 2002. Surfactants and Polymers in Aqueous Solution. Wiley-Blackwell. https://doi.org/10.1002/0470856424.

Huppert, H.E., Neufeld, J.A., Strandkvist, C., 2013. The competition between gravity and flow focusing in two-layered porous media. J. Fluid Mech. 720, 5–14. https://doi.org/10.1017/jfm.2012.623.

Jawitz, J.W., Annable, M.D., Rao, P.S.C., 1998. Miscible fluid displacement stability in unconfined porous media: two-dimensional flow experiments and simulations. J. Contam. Hydrol. 31, 211–230. https://doi.org/10.1016/S0169-7722(97)00062-4.

Jin, M., Hirasaki, G.J., Jackson, R.E., Kostarelos, K., Pope, G.A., 2007. Control of downward migration of dense nonaqueous phase liquid during surfactant flooding by design simulations. Water Resour. Res. 43 https://doi.org/10.1029/2006WR004858.

Kibbey, T.C.G., Ramsburg, C.A., Pennell, K.D., Hayes, K.F., 2002. Implications of alcohol partitioning behavior for *in situ* density modification of entrapped dense nonaqueous phase liquids. Environ. Sci. Technol. 36, 104–111. https://doi.org/10.1021/es010966q.

Kono, H., 2014. Characterization and properties of carboxymethyl cellulose hydrogels crosslinked by polyethylene glycol. Carbohydr. Polym. 106, 84–93. https://doi.org/10.1016/j.carbpol.2014.02.020.

Koohbor, B., Fahs, M., Ataie-Ashtiani, B., Belfort, B., Simmons, C.T., Younes, A., 2019. Uncertainty analysis for seawater intrusion in fractured coastal aquifers: effects of fracture location, aperture, density and hydrodynamic parameters. J. Hydrol. 571, 159–177. https://doi.org/10.1016/j.jhydrol.2019.01.052 (Amst).

Lee, M., Kang, H., Do, W., 2005. Application of nonionic surfactant-enhanced *in situ* flushing to a diesel contaminated site. Water Res. 39, 139–146. https://doi.org/10.1016/j.watres.2004.09.012.

Lenormand, R., Touboul, E., Zarcone, C., 1988. Numerical models and experiments on immiscible displacements in porous media. J. Fluid Mech. 189, 165–187. https://doi.org/10.1017/S0022112088000953.

Longo, S., Ciriello, V., Chiapponi, L., Di Federico, V., 2015. Combined effect of rheology and confining boundaries on spreading of gravity currents in porous media. Adv. Water Resour. 79, 140–152. https://doi.org/10.1016/j.advwatres.2015.02.016.

Longpré-Girard, M., Martel, R., Robert, T., Lefebvre, R., Lauzon, J.M., Thomson, N., 2020. Surfactant foam selection for enhanced light non-aqueous phase liquids (LNAPL) recovery in contaminated aquifers. Transp. Porous Media 131, 65–84.

Lunn, S.R.D., Kueper, B.H., 1999. Manipulation of density and viscosity for the optimization of DNAPL recovery by alcohol flooding. J. Contam. Hydrol. 38, 427–445. https://doi.org/10.1016/S0169-7722(99)00008-X.

Maire, J., Davarzani, H., Colombano, S., Fatin-Rouge, N., 2019. Targeted delivery of hydrogen for the bioremediation of aquifers contaminated by dissolved chlorinated compounds. Environ. Pollut. 249, 443–452. https://doi.org/10.1016/j.envpol.2019.03.033.

Mansouri-Boroujeni, M., Soulaine, C., Azaroual, M., Roman, S., 2023. How interfacial dynamics controls drainage pore-invasion patterns in porous media. Adv. Water. Resour. 171, 104353 https://doi.org/10.1016/j.advwatres.2022.104353.

Martel, K.E., Martel, R., Lefebvre, R., Gélinas, P.J., 1998. Laboratory study of polymer solutions used for mobility control during *in situ* NAPL recovery. Groundw. Monit. Remediat. 18, 103–113. https://doi.org/10.1111/j.1745-6592.1998.tb00734.x.

Martel, R., Hébert, A., Lefebvre, R., Gélinas, P., Gabriel, U., 2004. Displacement and sweep efficiencies in a DNAPL recovery test using micellar and polymer solutions injected in a five-spot pattern. J. Contam. Hydrol. 75, 1–29. https://doi.org/10.1016/j.jconhyd.2004.03.007.

Miller, C.T., Hill, E.H., Moutier, M., 2000. Remediation of DNAPL-contaminated subsurface systems using density-motivated mobilization. Environ. Sci. Technol. 34, 719–724.

Najjari, M.R., Hinke, J.A., Bulusu, K.V., Plesniak, M.W., 2016. On the rheology of refractive-index-matched, non-Newtonian blood-analog fluids for PIV experiments. Exp. Fluids 57, 1–6. https://doi.org/10.1007/S00348-016-2185-X/FIGURES/4.

O'Carroll, D., Sleep, B., Krol, M., Boparai, H., Kocur, C., 2013. Nanoscale zero valent iron and bimetallic particles for contaminated site remediation. Adv. Water Resour. 51, 104–122. https://doi.org/10.1016/J.ADVWATRES.2012.02.005.

Omirbekov, S., Colombano, S., Alamooti, A., Batikh, A., Cochennec, M., Amanbek, Y., Ahmadi-Senichault, A., Davarzani, H., 2023. Experimental study of DNAPL displacement by a new densified polymer solution and upscaling problems of aqueous polymer flow in porous media. J. Contam. Hydrol. 252, 104120 https://doi.org/10.1016/j.jconhyd.2022.104120.

Pennell, K.D., Abriola, L.M., 2017. Surfactant-enhanced aquifer remediation: fundamental processes and practical applications. Fundamentals and Applications. Routledge, pp. 693–750.

Pennell, K.D., Pope, G.A., Abriola, L.M., 1996. Influence of viscous and buoyancy forces on the mobilization of residual tetrachloroethylene during surfactant flushing. Environ. Sci. Technol. 30, 1328–1335. https://doi.org/10.1021/es9505311.

Philippe, N., Davarzani, H., Colombano, S., Dierick, M., Klein, P.Y., Marcoux, M., 2020. Experimental study of the temperature effect on two-phase flow properties in highly permeable porous media: application to the remediation of dense non-aqueous phase liquids (DNAPLs) in polluted soil. Adv. Water. Resour. 146, 103783 https://doi.org/10.1016/j.advwatres.2020.103783.

Ramsburg, C.A., Pennell, K.D., 2002. Density-modified displacement for dense nonaqueous-phase liquid source-zone remediation: density conversion using a partitioning alcohol. Environ. Sci. Technol. 36, 2082–2087. https://doi.org/10.1021/es011357l.

Robert, T., Martel, R., Conrad, S.H., Lefebvre, R., Gabriel, U., 2006. Visualization of TCE recovery mechanisms using surfactant-polymer solutions in a two-dimensional heterogeneous sand model. J. Contam. Hydrol. 86, 3–31. https://doi.org/10.1016/j.jconhyd.2006.02.013.

Rochefort, W.E., Middleman, S., 2000. Rheology of xanthan gum: salt, temperature, and strain effects in oscillatory and steady shear experiments. J. Rheol. 31, 337. https://doi.org/10.1122/1.549953 (N. Y. N. Y).

Rodrigues, R., Betelu, S., Colombano, S., Masselot, G., Tzedakis, T., Ignatiadis, I., 2017. Influence of temperature and surfactants on the solubilization of hexachlorobutadiene and hexachloroethane. J. Chem. Eng. Data 62, 3252–3260. https://doi.org/10.1021/acs.jced.7b00320.

Santos, A., Fernández, J., Guadaño, J., Lorenzo, D., Romero, A., 2018. Chlorinated organic compounds in liquid wastes (DNAPL) from lindane production dumped in landfills in Sabiñanigo (Spain). Environ. Pollut. 242, 1616–1624. https://doi.org/10.1016/J.ENVPOL.2018.07.117.

Shook, G.M., Pope, G.A., Kostarelos, K., 1998. Prediction and minimization of vertical migration of DNAPLs using surfactant enhanced aquifer remediation at neutral buoyancy. J. Contam. Hydrol. 34, 363–382. https://doi.org/10.1016/S0169-7722(98)00090-4.

Taghavy, A., Costanza, J., Pennell, K.D., Abriola, L.M., 2010. Effectiveness of nanoscale zero-valent iron for treatment of a PCE–DNAPL source zone. J. Contam. Hydrol. 118, 128–142. https://doi.org/10.1016/J.JCONHYD.2010.09.001.

Taylor, T.P., Pennell, K.D., Abriola, L.M., Dane, J.H., 2001. Surfactant enhanced recovery of tetrachloroethylene from a porous medium containing low permeability lenses: 1. Experimental studies. J. Contam. Hydrol. 48, 325–350. https://doi.org/10.1016/S0169-7722(00)00185-6.

Taylor, T.P., Rathfelder, K.M., Pennell, K.D., Abriola, L.M., 2004. Effects of ethanol addition on micellar solubilization and plume migration during surfactant enhanced recovery of tetrachloroethene. J. Contam. Hydrol. 69, 73–99. https://doi.org/10.1016/S0169-7722(03)00151-7.

Tsakiroglou, C.D., Sikinioti-Lock, A., Terzi, K., Theodoropoulou, M., 2018. A numerical model to simulate the NAPL source zone remediation by injecting zero-valent iron nanoparticles. Chem. Eng. Sci. 192, 391–413. https://doi.org/10.1016/J.CES.2018.07.037.

Walker, D.I., Cápiro, N.L., Chen, E., Anderson, K., Pennell, K.D., 2022. Micellar solubilization of binary organic liquid mixtures for surfactant enhanced aquifer remediation. J. Surfactants Deterg. 26 (3), 357–368. https://doi.org/10.1002/jsde.12637.

Wu, W., Delshad, M., Oolman, T., Pope, G.A., 2000. Remedial options for creosote-contaminated sites. Groundw. Monit. Remediat. 20, 78–86. https://doi.org/10.1111/j.1745-6592.2000.tb00268.x.

Yang, C., Offiong, N.A., Chen, X., Zhang, C., Liang, X., Sonu, K., Dong, J., 2020. The role of surfactants in colloidal biliquid aphrons and their transport in saturated porous medium. Environ. Pollut. 265, 114564 https://doi.org/10.1016/J.ENVPOL.2020.114564.

Yan, Y.L., Deng, Q., He, F., Zhang, X.Q., Liu, Y.P., 2011. Remediation of DNAPL-contaminated aquifers using density modification method with colloidal liquid aphrons. Colloids. Surf. A Physicochem. Eng. Asp. 385, 219–228. https://doi.org/10.1016/j.colsurfa.2011.06.012.

Yuan-Hui, L., Gregory, S., 1974. Diffusion of ions in sea water and in deep-sea sediments. Geochim. Cosmochim. Acta 38, 703–714. https://doi.org/10.1016/0016-7037(74)90145-8.

Zamani, N., Bondino, I., Kaufmann, R., Skauge, A., 2015. Effect of porous media properties on the onset of polymer extensional viscosity. J. Pet. Sci. Eng. 133, 483–495. https://doi.org/10.1016/j.petrol.2015.06.025.

Zheng, Z., Soh, B., Huppert, H.E., Stone, H.A., 2013. Fluid drainage from the edge of a porous reservoir. J. Fluid Mech. 718, 558–568.

Zhong, L., Oostrom, M., Wietsma, T.W., Covert, M.A., 2008. Enhanced remedial amendment delivery through fluid viscosity modifications: experiments and numerical simulations. J. Contam. Hydrol. 101, 29–41.